Nuclear level density: Shell-model approach

Roman Sen'kov[1,*] and Vladimir Zelevinsky[2,†]
[1]*Department of Natural Sciences, LaGuardia Community College, City University of New York, 31-10 Thomson Avenue, Long Island City, New York 11101, USA*
[2]*Department of Physics and Astronomy and National Superconducting Cyclotron Laboratory, Michigan State University, East Lansing, Michigan 48824-1321, USA*
(Received 14 August 2015; revised manuscript received 14 April 2016; published 6 June 2016)

Knowledge of the nuclear level density is necessary for understanding various reactions, including those in the stellar environment. Usually the combinatorics of a Fermi gas plus pairing is used for finding the level density. Recently a practical algorithm avoiding diagonalization of huge matrices was developed for calculating the density of many-body nuclear energy levels with certain quantum numbers for a full shell-model Hamiltonian. The underlying physics is that of quantum chaos and intrinsic thermalization in a closed system of interacting particles. We briefly explain this algorithm and, when possible, demonstrate the agreement of the results with those derived from exact diagonalization. The resulting level density is much smoother than that coming from conventional mean-field combinatorics. We study the role of various components of residual interactions in the process of thermalization, stressing the influence of incoherent collision-like processes. The shell-model results for the traditionally used parameters are also compared with standard phenomenological approaches.

DOI: 10.1103/PhysRevC.93.064304

I. INTRODUCTION

Knowledge of the level density is an important element in understanding the behavior of a quantum many-body system of interacting particles in various physical processes. In nuclear physics, this knowledge is necessary for the description of numerous reactions, including those of astrophysical or technological interest. Cross sections can be very sensitive to the level density, that typically grows exponentially as a function of the excitation energy and the number of constituents. In turn, the theoretically predicted level density is sensitive to the statistics of particles, their specific interactions, and available orbital space that, in realistic computation, usually has to be truncated. Apart from that, the level density in a finite self-bound system, such as the atomic nucleus, can be different for the available classes of eigenstates characterized by different quantum numbers of exact constants of motion (in nuclei total spin J, parity Π if we neglect weak interaction, and isospin T if we neglect interactions violating charge independence).

Below we consider a problem of practical microscopic calculation of the level density for a nucleus described by a Hamiltonian of the shell-model type. In this framework it does not matter if the Hamiltonian is derived from a more fundamental approach or fit phenomenologically with the use of experimental data. We assume that the Hamiltonian describes the low-lying energy spectra, transition rates, and other observables known from experiments reasonably well. Then the task is to predict the level density of the system at higher excitation energy, in the region beyond direct measurements resolving individual quantum states. Practically, the relevant factual milestones, apart from the low-lying spectroscopy, are the regions of isolated neutron resonances near neutron separation energy and the results of the Oslo method and related experimental approaches [1–4]. Of course, any practical shell-model Hamiltonian loses its validity outside of the truncated orbital space where this Hamiltonian was expected to work. At some excitation energy, the states of the system come from the particle orbitals not included in the model. However, with available computational means, the space of validity of the model Hamiltonian can be broad enough, in particular including the excited states involved; for example, in astrophysical reactions at a typical stellar temperature. We can also hope to use the microscopic results for the nuclei far from stability, where the level density is usually predicted by pure phenomenology [5].

Another physical limitation arises from the obvious fact that the states involved in the reactions belong to the continuum, while the standard shell-model calculations work in the discrete spectrum. Instead of discrete states, here one has to deal with resonances seen in various reactions. Then the whole definition of the level density becomes questionable and, strictly speaking, one has to move to the complex plane of resonances. However, the traditional approach is still meaningful if the typical widths of the involved states are small compared to the spacings between the states with the same quantum numbers. In what follows we limit ourselves to this situation.

Neglecting the continuum effects, the trivial solution for the level density generated by a certain Hamiltonian would be a full diagonalization of the Hamiltonian matrix in an appropriate orbital basis. However, this is practically only possible in sharply truncated orbital spaces, which might be only sufficient for relatively light nuclei, such as those in the *sd* shell [6]. In many realistic cases of current interest, the dimensions of corresponding matrices, even in subspaces with given quantum numbers, are prohibitively large. Moreover, such a diagonalization is anyway superfluous because we

*rsenkov@lagcc.cuny.edu
†zelevins@nscl.msu.edu

do not need full information on every excited state in spectral regions of high level density. The level density is, by construction, a statistical notion.

In this situation, we are looking for the statistical solution of the problem. The physical justification of such an approach lies in the fact that, at small level spacings, the stationary nuclear states are extremely complicated superpositions of simple determinantal states with integer occupation numbers of definite orbitals. Gradually switching on inter-particle interactions and going in this process through multiple avoided crossings of various configurations we come to *chaotic* states [6,7] with observable properties smoothly changing along the spectrum. Therefore our problem reduces to finding a realistic way to describe this smooth evolution.

This goal can be reached using the methods of *statistical nuclear spectroscopy* [8–10]. Already in the framework of a single partition (a certain configuration of independent particles occupying the mean field levels), the level density after including the particle interaction rapidly goes to the Gaussian limit with increasing particle number [11]. This is some kind of manifestation of the central limit theorem. The many-level, and therefore many-partition, generalization should give a reliable image of the total level density for an accepted orbital scheme. This has to be done for each class of global quantum numbers. This direction of theoretical search has a long history. We would like to especially mention the works in the direction of statistical spectroscopy applied to shell-model Hamiltonians; see for example [12,13]. After several preliminary publications, our successful algorithm was constructed [14] and opened for public use [15]. The results of implementing this algorithm for the level density in sectors with given values of global constants of motion are practically identical to those from the full diagonalization when the latter is possible. For well-tested shell-model Hamiltonians, the results are in good agreement with available experimental data.

For many years, starting with the classic work by Bethe [16], the nuclear level density was estimated using combinatorics based on the ideas of a Fermi gas. An influential review of earlier approaches of this type was given by Ericson [17], and later derivations can be found in [18–21]; see also [22]. Recent achievements in this direction [23–25] include the pairing correlations considered as a part of the self-consistent mean field in the framework of the BCS theory or Hartree-Fock-Bogoliubov variational ansatz. The shell-model Monte Carlo methods [26–28], being very demanding computationally, work relatively well, at least with some parts of the full shell-model interaction, but require the projection to the correct values of spin and parity.

The chaotization of the dynamics mentioned above leads to the possibility of describing the physics of excited states at high level density in terms of statistical thermodynamics including temperature, entropy, etc. This was understood in the application to nuclear reactions from the early times of nuclear physics [16,29,30]. Detailed analysis of atomic [31,32] and nuclear [6,33] chaotic states supported an old idea [34] of thermalization in a closed system driven by the interactions between the constituents, with no heat bath: the average over a generic chaotic wave function in a chaotic region is equivalent to the average over a standard equilibrium thermal ensemble [35]. Currently this idea, sometimes called the "eigenfunction thermalization hypothesis," is extensively discussed in the many-body physics community [36]. One of the purposes of the current publication is to compare the exact shell-model nuclear level density with phenomenological ideas based on the Fermi-gas picture at a certain temperature. We look at these ideas and, based on them, equations from the viewpoint of our numerical results. Our attention will be mostly concentrated on the usually cited empirical parameters of the level density and their energy and spin dependence. Another point of interest is in the role of various components of the shell-model interactions in the formation of the level density. One important result is that the consideration of the mean field, even with addition of the BCS-type pairing, is not sufficient. Incoherent components of the interaction in a finite many-body system, as a rule neglected in the mean-field combinatorics, play a significant role in smoothing the energy behavior of the level density.

In what follows we briefly explain the method and give examples of practical calculations. The results will be compared with what would follow from traditional phenomenological models.

II. MOMENTS METHOD

We consider a finite system of interacting fermions described by the standard Hamiltonian

$$H = \sum_{1} \epsilon_1 a_1^\dagger a_1 + \frac{1}{4} \sum_{1234} V_{12;34} a_1^\dagger a_2^\dagger a_3 a_4 \qquad (1)$$

that contains the mean-field part with effective single-particle energies ϵ_1 and the antisymmetrized two-body interaction. The generalized numerical subscripts combine all quantum numbers of single-particle orbitals. In this form the method can be applied to nuclei, atomic or molecular electrons, atoms in traps, etc.; any system where the residual interaction is sufficiently strong to produce complicated eigenstates. The three-body forces can be included in the same way, although the computations become more cumbersome. Using a phenomenological shell-model Hamiltonian we assume that many-body forces, at least partly, are included in fitted matrix elements. The quality of the Hamiltonian is checked by the explicit applications to individual low-lying states and comparison with available experimental information.

In a finite self-bound system, such as the atomic nucleus, the total angular momentum (nuclear spin) is exactly conserved, supplying good global quantum numbers J and M. Therefore it is convenient from the very beginning to use a spherically symmetric basis of single-particle orbitals $|jm)$ which define, along with the orbital momentum ℓ, main quantum number ν and isospin τ, the quantum numbers combined in Eq. (1) into a unified numerical subscript. If the orbital space is sufficiently broad, this spherical shell model can describe intrinsic deformation without violating rotational symmetry [37]. In practice, the operators in the Hamiltonian can be combined into pairs, such as $(a_3 a_4)_{L\Lambda}$, with the angular momentum quantum numbers of the pair, $L\Lambda$, fixed through the Clebsch-Gordan coefficients. In the same way, for the

isospin-invariant forces, the isospin of the pair can be also fixed, and then the interaction V in a restricted orbital space is defined through a finite number of pairwise matrix elements. If more convenient for computations, one can as well use the M scheme without vector coupling.

The practical algorithm of calculations in the M scheme follows from individual configurations, p (*partitions*), which are possible distributions $(n_1,n_2,\dots)$ of available N particles over single-particle orbitals (here the index 1 does not include the projection m). The many-body states $|\alpha\rangle$ possible for each partition form a subspace where α combines total quantum numbers N,M,T_3 and parity. It is convenient [14] to use the proton-neutron formalism.

Let $D_{\alpha p}$ be the dimension of the class of states with global quantum numbers α built on the partition p. As shown in statistical spectroscopy [9,11] and confirmed in many examples by the exact shell-model diagonalization, the density of states for a given partition is close to Gaussian. Of course, this is the main assumption based on a rich experience with the features of quantum chaos in mesoscopic systems. The characteristics of the Gaussian are defined by the moments (traces) of the actual Hamiltonian. The centroid is just the mean energy value for a given partition,

$$E_{\alpha p} = \langle H\rangle_{\alpha p} = \frac{1}{D_{\alpha p}}\,\mathrm{Tr}^{(\alpha p)} H. \tag{2}$$

The dispersion of the Gaussian, $\sigma_{\alpha p}$, is the second moment,

$$\sigma^2_{\alpha p} = \langle H^2\rangle_{\alpha p} - E^2_{\alpha p} \equiv \frac{1}{D_{\alpha p}}\,\mathrm{Tr}^{(\alpha p)} H^2 - E^2_{\alpha p}. \tag{3}$$

It is important to stress that the calculation of these traces does not require the diagonalization of large-scale matrices. The first moment (2) is the diagonal matrix element of the Hamiltonian averaged over the partition, while the second moment (3) is the sum of squared off-diagonal elements along one line of the Hamiltonian matrix, again averaged over the lines corresponding to the partition. It is known that the dispersion for each basis state very weakly fluctuates within a partition [6,38] even prior to the next averaging. The second moment includes all interactions coupling the partitions. If the traces were calculated in the M scheme, we obtain the *density of states* counting all M-degenerate states within the multiplets. To obtain the *level density* for given spin J, we have to find in a standard way the difference of traces for $M = J$ and $M = J + 1$.

The total level density is given by summing the contributions of partitions using the constructed Gaussians $G_{\alpha p}(E)$ with their centroids (2) and widths (3):

$$\rho(E;\alpha) = \sum_p D_{\alpha p} G_{\alpha p}(E). \tag{4}$$

As was understood earlier [39], it is better to use *finite range Gaussians*,

$$G_{\alpha p}(E) = G(E - E_{\alpha p} + E_{\mathrm{g.s.}};\sigma_{\alpha p}), \tag{5}$$

where

$$G(x;\sigma) = \mathcal{C}\begin{cases} e^{-x^2/2\sigma^2}, & |x| \leqslant \eta\sigma, \\ 0, & |x| > \eta\sigma. \end{cases} \tag{6}$$

Here $E_{\mathrm{g.s.}}$ is the ground state energy to be defined separately, $\mathcal{C}$ is the normalizing factor, $\int dx\, G(x,\sigma) = 1$, and the cutting finite-range parameter η has to be found empirically [40]; its actual value $\eta \approx 2.8$ agrees with the analysis of the shape of typical nuclear strength functions [41].

Following the recipe of Ref. [42] we make an important addition to the algorithm. In many realistic applications, the orbital space contains several shells labeled by the harmonic oscillator quanta $\mathcal{N}$. In this case, the standard formulation of the shell model with cross-shell transitions includes unphysical excitations of the center of mass. These spurious states are to be excluded from the level density. In some versions of the shell model, these states are artificially shifted to high energies. Here, the subtraction of ghost states is accomplished by renormalizing the contaminated level density $\rho(E,J;\mathcal{N})$ through the recurrence relations. For example, while the $\mathcal{N} = 0$ case, which will be called the $\rho^\circ(E,J;0)$ approximation, is free of admixtures, the pure level density ρ° at the next step (no admixtures of the single center-of-mass excitation) is found as

$$\rho^\circ(E,J;1) = \rho(E,J;1) - \sum_{J'\leqslant|J-1|}^{J+1} \rho(E,J';0). \tag{7}$$

Here the sum goes over the intermediate angular momenta J' from $|J-1|$ to $J+1$ since the center-of-mass operator is equivalent to a vector. If higher admixtures $\mathcal{N} > 1$ are present, the recurrence relation has to include a corresponding number of steps back. This makes the calculation of the trace of H^2 with various intermediate states slightly more involved [40,43].

III. EXAMPLES OF LEVEL DENSITY

A. Comparison with the exact solution of the shell model

The first natural check of the approach is in comparison of the resulting level density with the picture arising from the full shell-model diagonalization in the cases where such a diagonalization is technically plausible. The sd-shell model for a long time has been known as the best example of exact diagonalization. The model is completely fixed by the effective single-particle energies $d_{5/2}$, $s_{1/2}$, and $d_{3/2}$ and 63 phenomenologically fitted matrix elements of two-body interaction. The model works extremely well for practically all observables of sd nuclei and not only for the lowest states. For example, both the experiment [44] and the sd-shell model [42] indicate the existence of ten stationary states with $J^\Pi = 0^+$ up to an excitation energy of 15 MeV in ^{28}Si, therefore providing the same average level density, at least at not very high energy; the mean level spacing between those 0^+ levels is 0.95 MeV in the experiment and 1.02 MeV in the shell-model calculation.

Figure 1 illustrates the results of the moments method for calculating the level density in ^{24}Mg (see also Fig. 1 in Ref. [40] for similar results in ^{28}Si, a typical object of sd-shell model applications that served long ago as a testing ground for quantum chaos [6]). The level density for different classes of states, here 0^+, 1^+, 2^+, and 3^+, is always a smooth curve of Gaussian type. Of course, as the calculations have been done in the restricted orbital space, the real physical result that can be juxtaposed to the experimental data and used for the reaction

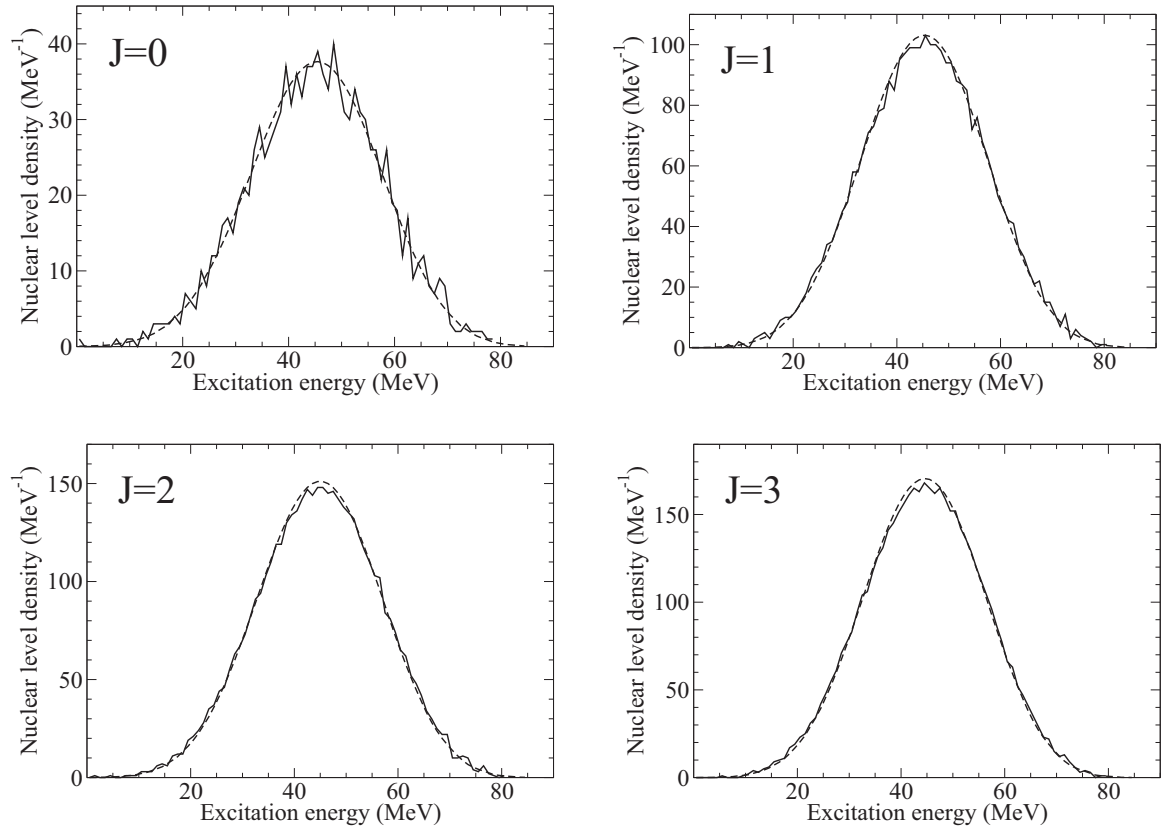

FIG. 1. Nuclear level densities for ^{24}Mg, $\Pi = +1$ and various spins, for the sd-shell and USDB two-body interaction [45]; full shell-model diagonalization (solid curves) vs moments method (dashed curves); finite-range parameter $\eta = 2.7$.

calculations always corresponds only to the left-hand side of the full graph and to the excitation energy below the centroid maximum.

Various specific quantum numbers (total spin, except for the maximal one, and parity) produce a level density of the same qualitative behavior, with the integral corresponding to exact multiplicities of states with a given set of quantum numbers in a fixed orbital space. All examples look the same. The agreement with the exact shell-model diagonalization is almost perfect, with slightly more visible fluctuations for the class $J^{\Pi} = 0^{+}$ that has a smaller total dimension. In all cases we see a small deviation near the centroid, which supposedly can be eliminated by taking into account the fourth moment of the Hamiltonian (but it makes no sense to go for such complicated and time-consuming calculations to improve the results in the region outside the physically relevant area). In the cases of the shell model with cross-shell transitions, the removal of the spurious states restores the symmetry of the level density and makes the calculation of the third moment unnecessary.

The smoothness and Gaussian behavior of results in all cases confirm the possible thermodynamic interpretation in terms of entropy $S(E)$ (mean logarithm of the level density) and temperature, $dS/dE = 1/T(E)$. Formally, the centroid of the level density for the finite orbital space corresponds to infinite temperature and the right half of the curve to negative temperatures. The full shell-model analysis of the wave functions [6] has found that the same effective temperature can be extracted by a single-particle thermometer using the occupation numbers of available spherical orbitals *for individual stationary many-body states*. The interaction of the quasiparticles in the self-consistent mean field acts as the heat bath, and the chaotic mixing of the eigenstates leads to thermalization even in such a small Fermi system.

B. Elimination of spurious states

As mentioned above, the full shell-model diagonalization in the cases with the presence of transitions between the orbitals of opposite parity (excitations across the oscillator shells) brings in ghost states related to the center-of-mass motion rather than to intrinsic excitations. We explained above the recurrent techniques used for eliminating these spurious states and obtaining the pure level density. The recipe frequently used in the shell model is the brute-force shift of the undesired states to high energy by adding to the Hamiltonian under diagonalization a Lawson term [46] that in the harmonic oscillator field of frequency ω looks like ($\beta > 0$)

$$H' = \beta\left[H_{\text{c.m.}} - \frac{3}{2}\hbar\omega\right]\frac{A}{\hbar\omega}. \tag{8}$$

As was shown long ago [6], this recipe indeed generates a new branch of eigenstates shifted to high energy (by about $\sim\beta\mathcal{N}A$) but having essentially the same complexity (measured by the information entropy) as their predecessors without spurious admixtures. The separation of unphysical spurious states

according to the recurrence relations (7) works very well; for more details and examples see Ref. [14].

IV. SHELL-MODEL PREDICTIONS AND MEAN-FIELD COMBINATORICS

The widely used standard road to the nuclear level density is going through the mean-field representation of the nuclear dynamics. This traditional approach is based on the classical idea [16,17] of a Fermi gas, where the excited levels result from combinations of many particle-hole excitations. Practically, the combinatorics used single-particle excitations from the fully occupied Fermi surface identified with the ground state population of the lowest individual orbitals. At low excitation energy, a renormalization of the level density is related to the gap due to the Cooper pairing. In complex nuclei, the low-energy levels observed inside the gap can be interpreted as collective excitations, vibrational and/or rotational. As the collective phenomena of these types correspond typically to the slow self-consistent motion of many particles, it is natural to expect that such coherent combinations of single-particle excitations partly compensate the deficit of levels at low energy due to the pairing gaps and give rise to the so-called *collective enhancement* of the level density [22,48] in comparison to the single-particle combinatorics of independent particles and holes. Modern refined approaches of this class account in various forms for the pairing phenomenon that changes the excitation spectrum, especially in even-even nuclei [23–25].

In the spirit of mean-field combinatorics, one has to expect the corresponding suppression of level density at higher excitation energy (damping of collective enhancement); the level density is just redistributed. When the general level density grows, the vibrational modes become strongly mixed with simpler excitations of the two-quasiparticle and more complicated structures, as is known very well from the widths of the giant resonances. With smoothing shell gaps, it is harder to distinguish between rotational and intrinsic motion. Recent experiments in nuclei, where low-lying collective excitations are well known, did not find clear phenomena of collective enhancement and its fade-out [49].

In not too heavy nuclei, the quasiparticle combinatorics (on the base of the BCS or Hartree-Fock-Bogoliubov pairing description) reveals stepwise effects of subshell occupation and pair breaking. This leads, at relatively low energy, to the irregular picture of the level density that clearly reflects these steps. The shell-model Hamiltonians, as a rule, contain all interaction matrix elements allowed by the selection rules. One of the main conclusions of the full shell-model calculation is that the presence of all interactions is significantly smoothing the whole picture so that it is hard to see the traces of individual families which could be still recognized only by the special observables and selection rules for the individual transitions. We can recall that our algorithm still starts with the partitions formed by independent particles, which then overlap and lose their boundaries.

The shell-model Hamiltonian contains all pairing matrix elements (and not in the simplified form with constant matrix elements) as well as the interaction processes responsible for multipole-multipole forces and deformation. Therefore all collective effects are fully taken into account if the orbital space is sufficiently broad. Figure 2 shows the comparison of the level densities in the nucleus ^{64}Ge (see also Figs. 4 and 5 in [40] for similar results in ^{54}Fe and ^{52}Cr nuclei). The thin dotted lines give the level density found with the mean-field combinatorics built on the Hartree-Fock mean field and BCS pairing. All irregularities found through the mean-field combinatorics are completely smoothed in the full moments calculation. This is a typical result encountered in all examples. Again we see that the method under discussion produces a level density practically identical to the full shell-model diagonalization when the latter is possible. One can note that the shell-model and mean field approaches use different interactions. The shell-model parameters were fitted to describe well the low-energy data. We believe that the discrepancy between the shell-model and the mean field level densities has not accidental but qualitative character evident in all considered examples.

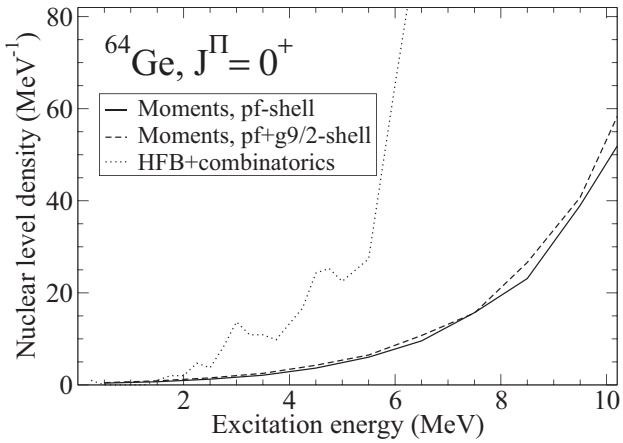

FIG. 2. Low-energy level density for ^{64}Ge, spin $J = 0$ and $\Pi = +1$. The solid curve presents the calculation in the pf shell with the GXPF1A interaction, the dashed curve corresponds to the calculation in the larger model space with the level $g_{9/2}$ added, and the dotted curve presents the results obtained using the HFB single-particle energies and the combinatorial method [47].

Using the moments method we can calculate nuclear level densities in very large model spaces, for example in the $pf + g_{9/2}$ model space. The interaction we used for this model space was built starting with the GXPF1A interaction for the pf model space, to which the G-matrix elements that describe the interaction between the pf shell and the $g_{9/2}$ orbit were added. The single-particle energy for the $g_{9/2}$ orbit was fixed at -0.637 MeV. Figures 2 and 3 present the level density of states 0^+ in the $N = Z$ nucleus ^{64}Ge calculated in the pf space (solid curves) and $pf + g_{9/2}$ shell (dashed curves); the dotted curve in Fig. 2 corresponds to HFB+combinatorial method. Figure 3 illustrates the influence of the enlargement of the orbital shell-model space [47]. The level density becomes sensitive to the inclusion of the next shell ($g_{9/2}$) only at excitation energy greater than 14 MeV, which means that the region of neutron resonances could be reliably evaluated with the more narrow orbital space. This case has important ramifications for the astrophysical consideration of element abundance since this

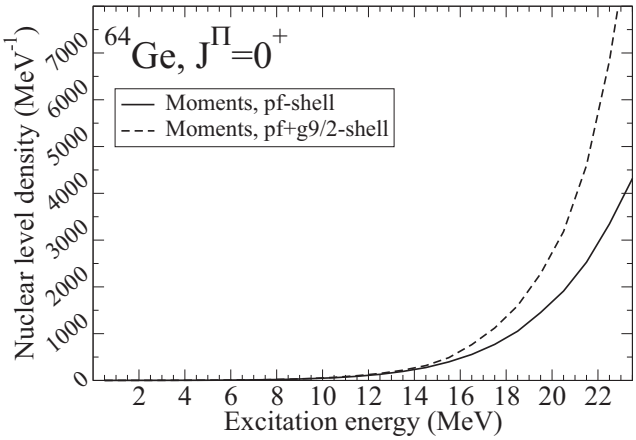

FIG. 3. Level density for ^{64}Ge, spin $J = 0$ and $\Pi = +1$. The densities are calculated in pf (solid curve) and in $pf + g_{9/2}$ (dashed curve) shells. The range of excitation energy is increased, compared to Fig. 3, up to 24 MeV.

nucleus is considered to be a waiting point in the r process of nucleosynthesis.

V. COHERENT AND INCOHERENT INTERACTIONS

As the whole shell-model Hamiltonian contributes to the traces defining the level density, we can explore the effects of individual components of the effective interactions, including the "incoherent" parts of the full Hamiltonian which do not significantly contribute to the formation of the mean field. These parts of the interaction determine the finite lifetime of the simple quasiparticle (or collective) modes and their fragmentation in terms of genuine complicated eigenstates of exceedingly entangled nature. In particular, these collision-like interactions are responsible for the formation of chaotic states with high information entropy and the process of thermalization [6]. For example, it was shown [50–52] that the exactly considered pairing interaction contains some chaotic features, but they are still not sufficient for establishing the complete chaotic picture comparable to the predictions of the Gaussian orthogonal ensemble.

Below we show the evolution of the level density as a function of the interaction modes included in the full calculation of the moments. Although it is not difficult to vary all individual matrix elements, here we use a simplified approach, presenting the whole two-body interaction Hamiltonian in the sd-shell model as consisting of two parts with variable intensity,

$$H = h + k_1 V(\text{pairing}) + k_2 V(\text{nonpairing}). \qquad (9)$$

Here h contains the single-particle energies, V(pairing) includes all matrix elements with the pairs of nucleons in the channel $J^{\pi}T = 0^{+}1$, while all other shell-model matrix elements are attributed to the last term. The numerical coefficients k_1 and k_2 are varied, giving rise to different versions of the shell model; the realistic case emerges at $k_1 = k_2 = 1$. It is easy to understand that in the moments method (and in the full diagonalization, see [6]) new independent components of the Hamiltonian add in quadratures to the final width of the shell-model level density.

The global evolution of the full level density in ^{28}Si, as the coefficients $k_1 = k_2$ are varied from 0.1 to their realistic values, is shown in the left graph of Fig. 4. The low residual interaction obviously keeps untouched the independent-particle partition structure of the Hilbert space that recalls the results of the mean-field combinatorics. As the parameters k_1,k_2 grow, the next curves show the development of the final picture. The configurational structure is gradually washed out by the residual interaction, leading to the final smooth level density discussed earlier. Let us stress that the observed evolution is not a consequence of the superposition of all subspaces with different values of J. The individual subspace $J^{\Pi} = 0^{+}$, the right graph on Fig. 4, demonstrates practically the same evolution.

Figure 5 describes the situation when the nonpairing components of interaction are suppressed, $k_2 = 0.1$, but the pairing strength evolves. Superposing all values of J (the left graph of Fig. 5), we see that the smooth Gaussian-like curve is achieved only at the nonrealistically high pairing strength. Again the picture is nearly the same when only the states $J = 0$

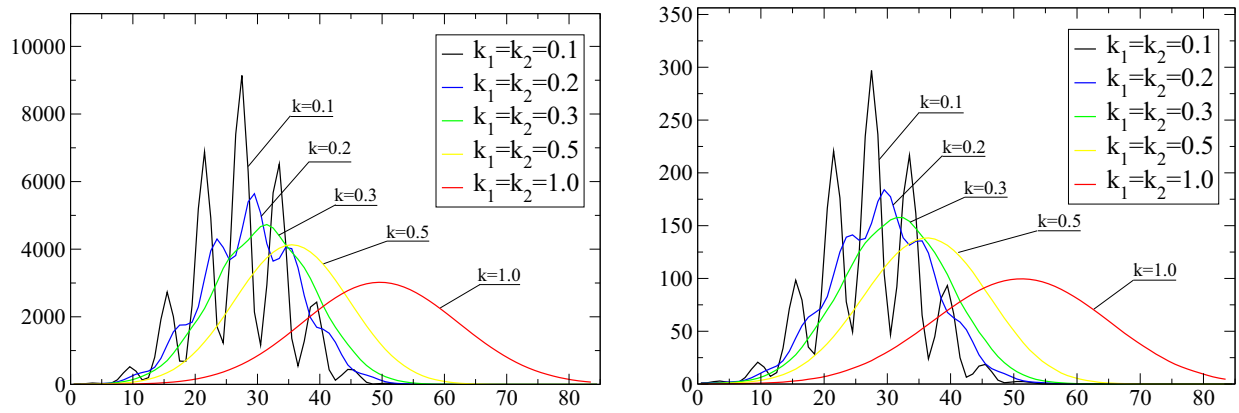

FIG. 4. Level density for ^{28}Si, sd model space. Different curves correspond to different scale factors of Eq. (9): $k_1 = k_2 = \{0.1, 0.2, 0.3, 0.5, 1.0\}$ when the pairing and nonpairing parts of the interaction scale similarly. The left graph corresponds to the total density with all J included, while the right graph describes the evolution of the $J = 0$ density.

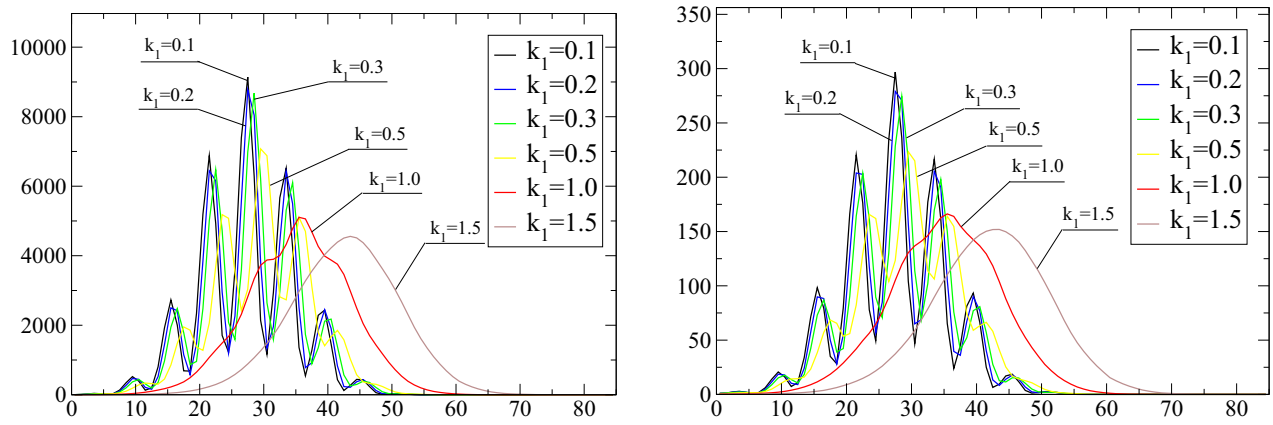

FIG. 5. Level density for ^{28}Si, *sd* model space. The nonpairing interaction is always turned off, $k_2 = 0.1$, while the pairing interaction scales are $k_1 = \{0.1,0.2,0.3,0.5,1.0,1.5\}$. The left graph corresponds to the total density with all J included, while the right graph describes the evolution of the $J = 0$ density.

are considered (the right graph of Fig. 5). The realistic pairing strength, $k_1 = 1.0$, at the absence of nonpairing interactions, is still not sufficient for the fully smooth level density. At low excitation energy <20 MeV the evolution of the level density for $J = 0$ clearly shows the disappearance of the typical large oscillations with the growth of pairing. Here, indeed, the pairing interaction shifts the noticeable part of levels to higher energies. If the pairing matrix elements are fixed at the empirical value, Fig. 6, the large bumps from the original partitions do not appear but the incoherent interactions very much broaden the final result. The generic character of this scenario is confirmed by Fig. 7 for ^{52}Fe.

VI. THERMODYNAMIC DESCRIPTION AND COMPARISON WITH PHENOMENOLOGY

A. Simple Fermi-gas

The shell-model Hamiltonian (1) starts from noninteracting particles or quasiparticles, elementary excitations in the mean field of a certain symmetry that determines the appropriate quantum numbers of excited states. For nuclei, an adequate image is that of the perfect two-component Fermi gas. The ground state of the system is the filled Fermi sphere, and the excited states are described by the particle-hole picture. In the realistic many-body physics, this is just an initial step that has to be followed by switching on the interaction between particles and holes. However, already at this stage, the level density increases exponentially, which justifies the traditional phenomenological approaches.

The particle-hole phenomenology uses the steepest descent method to calculate the level density as a function of excitation energy E through the Laplace transform of the partition function, which leads to the standard result for one type of particles,

$$\rho(E) = \frac{1}{4\sqrt{3}\,E}\, e^{2\sqrt{aE}}, \tag{10}$$

where the *level density parameter* is

$$a = \frac{\pi^2}{6}\, \nu_F \tag{11}$$

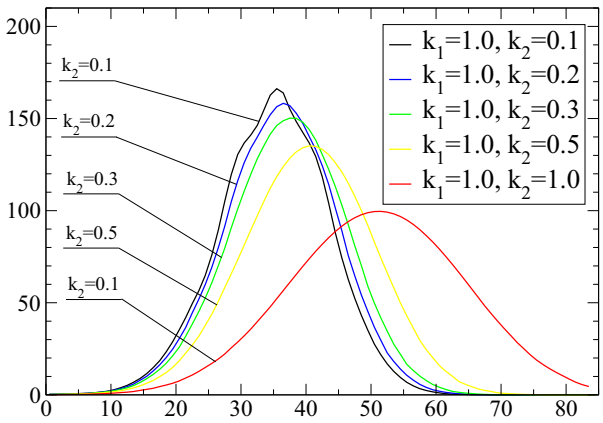

FIG. 6. Level density for ^{28}Si, $J = 0$, *sd* model space. The black curve presents $k_1 = 1.0, k_2 = 0.1$, then the remaining parts of the interaction are increased together with k_2 up to the red curve ($k_1 = k_2 = 1.0$) that describes the realistic interaction.

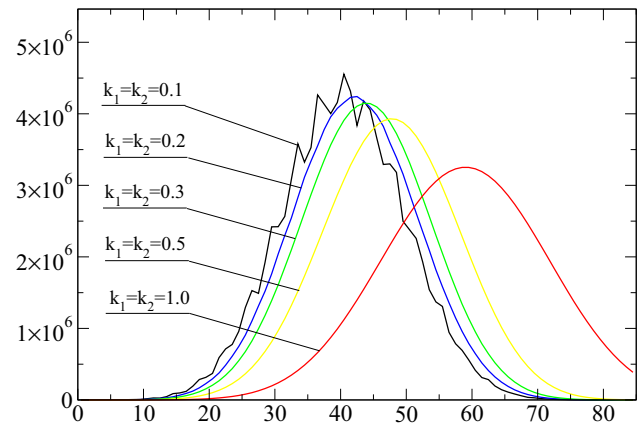

FIG. 7. Level density for ^{52}Fe, all J, pf model space. This figure and its color scheme are similar to the left panel of Fig. 4.

and ν_F is the density of *single-particle* states at the Fermi surface. The generalization to a proton-neutron system leads to a modified expression,

$$\rho(E) = \frac{\sqrt{\pi}\,\bar{a}}{12\,(aE)^{5/4}}\, e^{2\sqrt{aE}} = \frac{6^{1/4}\,\bar{\nu}}{12\,(\nu_F E)^{5/4}}\, e^{2\sqrt{aE}}, \quad (12)$$

where the parameters a and $\bar{a}$ now include the total single-particle density of states at the Fermi surface, $\nu_F = \nu_F(n) + \nu_F(p)$, and the effective single-particle density $\bar{\nu} = \nu_F^2/(2\sqrt{\nu_F(n)\nu_F(p)})$, correspondingly, see Eq. (11). The singularities at $E \to 0$ in densities (10) and (12) show that the statistical method of calculation is invalid at too low excitation energy where the number of nuclear many-body states is small. The notion of the level density requires that the excitation energy be greater than the average distance between the single-particle levels,

$$E \gg \frac{1}{\nu_F}. \quad (13)$$

In thermodynamic language, the nuclear temperature t is introduced through the Fermi-gas formula for the excitation energy,

$$E = at^2. \quad (14)$$

In general, for the low excitation energy region it is always recommended to use directly the available experimental information.

If one tries to compare the thermodynamic level density of Fermi-gas type with experimental data, it is hard to expect the numerical agreement of the level density parameter (11) with that required by data even if exponential growth of the total level density takes place. As mentioned in the Introduction, when the level density grows, the residual interactions lead to multiple avoided crossings and mixing of many-body levels with the same exact quantum numbers. This process of chaotization evolves the level network considered as a function of the interaction strength close to the aperiodic crystal with a small average spacing. The whole set of stationary states becomes locally close to the predictions of the Gaussian orthogonal ensemble of random matrices. The wave functions here are quite complicated superpositions of very many particle-hole states. The energy behavior of the level density is now close to a Gaussian [6], with a total width that is given by adding in quadrature the initial width due to the mean-field quasiparticles and the dispersion of the off-diagonal matrix elements of residual interactions.

Figure 8 shows the parameters a found from the shell-model calculation of the total level density $\rho(E)$ fitted by

$$\ln[\rho(E)] = 2\sqrt{aE} - \tfrac{5}{4}\ln E + \text{constant}. \quad (15)$$

To extract the parameter a we fit $(\ln[\rho(E)] + \frac{5}{4}\ln E)$ using a linear function of $\sqrt{E}$. As the result we get the slope $2\sqrt{a}$ and the intercept. The energy interval used for the interpolation should not start too low (it has to contain sufficiently many states and not go too far where the shell model does not work). For the fitted a parameters in Fig. 8 we used the energy interval from 5 to 25 MeV.

Both the parameter a and the *constant* show the change clearly correlated with the microscopic filling of the nuclear shells. The parameter a reveals the maximum in the middle of the shell occupation, as should have been expected from the construction of the model. This is the known Rosenzweig effect [55] described by Ericson [17] as due to "a considerably larger number of rearrangement possibilities when the shell is half-filled." The empirical estimates for the same nuclei are available from the level density at the neutron resonances energy [53] (these do not show considerable shell effects) and by extrapolation from low-lying levels [54] where one can see very weak shell effects in the region of the mass number around $A \approx 50$. The *constant* in Eq. (15) is small but also shows in some cases the shell-model dependence with a minimum in counter-phase with the parameter a. Extrapolations of the

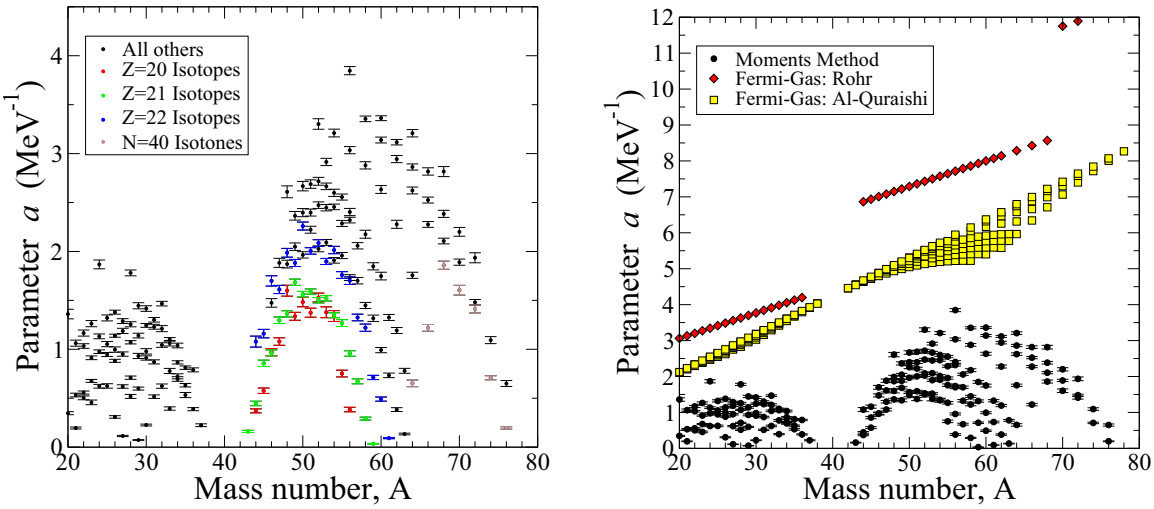

FIG. 8. Interpolation of the single-particle level density parameter a; see Eq. (15) and the details in the text. The fitting energy range is 5–25 MeV. Left panel: different colors present different isotopes or isotones. Right panel: moments-method calculation with interpolation (black circles), fit using the experimental data on neutron resonances (Ref. [53], red diamonds), and fit using experimental low-lying levels ([54], yellow squares).

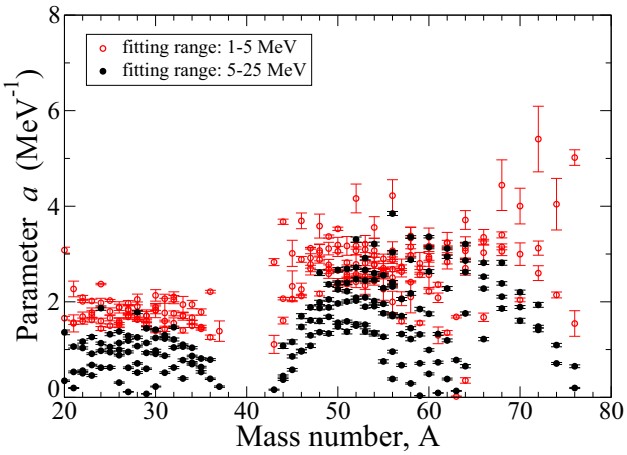

FIG. 9. Level density parameter (11) fitted in the simple Fermi-gas model for *sd* and *pf* shell nuclei. The empty circles (red color) present the fitting range 1-5 MeV and the filled black circles correspond to the fitting range 5–25 MeV. The error bars show the uncertainty of the level density parameter a due to the fitting.

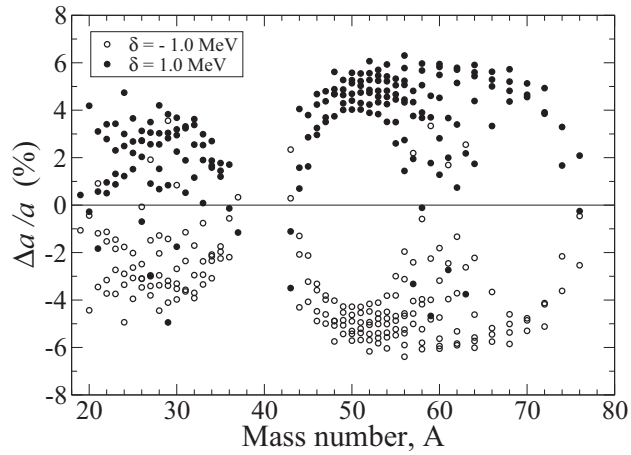

FIG. 10. The relative changes in the level density parameter a due to the pairing energy shift δ, Eq. (17), shown for *sd*- and *pf*-shell nuclei. The empty circles present the fit with the energy shift $\delta = -1$ MeV and the filled circles correspond to $\delta = 1$ MeV.

level density parameter a from low-lying levels and neutron resonances and from the shell-model approach use different energy intervals to fit the data; this could be one of the possible sources of a big discrepancy, but we agree that the question is far from being completely understood.

Figure. 9 shows the dependence of the level density parameter a on the energy range for which the fitting was performed. The empty circles (red color) present the low energy fit, around 1–5 MeV, while the filled circles (black color) present the standard 5–25 MeV energy range fit. We can see that at low energies the fitted level density parameter a is slightly larger, but still it is not large enough to be compared with the empirical estimates [53,54].

B. Back-shifted Fermi-gas model

In this paper we do not discuss in detail the nuclear pairing correlations and its importance for the nuclear level densities, leaving this for future consideration. One of the standard phenomenological ways to account for pairing correlation is to use the back-shifted Fermi-gas formula (BSFG) [18,56],

$$\rho_{\rm BSFG}(E) = \frac{\sqrt{\pi}\,\bar{a}}{12\,[a(E-\delta)]^{5/4}}\, e^{2\sqrt{a(E-\delta)}}, \qquad (16)$$

where the excitation energy is shifted by the pairing energy parameter δ. This introduces a new free parameter that should be fitted alongside the level density parameter a. The pairing energy parameter δ is in general different for even-even, odd-odd, and even-odd nuclei due to the formation of Cooper pairs, and does not necessarily coincide with the corresponding pairing gap parameters Δ or 2Δ.

Figure 10 shows the sensitivity of the level density parameter a to inclusion of the energy shift δ. The quantity plotted along y axis is the relative change in a if we shift the excitation energy by δ,

$$100\% \times \frac{a - a_{\rm BSFG}}{a}, \qquad (17)$$

where $a_{\rm BSFG}$ is the level density parameter fitted using Eq. (16) with a fixed value of the pairing energy δ. We can see that the a parameter varies only in a $\pm 6\%$ range when the shift changes from $\delta = -1$ MeV (presented by the empty circles) to $\delta = 1$ MeV (filled circles). We conclude that the inclusion of the pairing energy shift δ practically does not change the level density parameter a, instead it affects the *constant* in Eq. (15), which is not very interesting and can be fixed by the normalization.

C. Constant temperature model

The model of the energy dependence of the level density, different from the Fermi-gas phenomenology (12), was suggested long ago [18,56] and gradually has become popular among practitioners. It is assumed that the level density, at least up to 10 MeV excitation energy, and maybe even higher [57–59], can be described by the constant temperature T. This temperature is the single parameter defined, in the simplest version, according to the thermodynamics as

$$T = \left[\frac{d\ln\rho(E)}{dE}\right]^{-1}. \qquad (18)$$

The philosophy behind this approach is usually explained [60] in terms of the first-order phase transition that goes through the latent heat at fixed temperature. Although typically this assumes the melting of the Cooper pairs, in fact one can also talk about other types of correlated structures which are undergoing something similar to the liquid-gas phase transition or even the first stage on the road to multifragmentation. In a more detailed description, the effective temperature parameter can be different for the classes of states with different quantum numbers, although such a generalization does not seem applicable from the viewpoint of the thermal equilibrium between various degrees of freedom. Such an effective temperature parameter (plus a corresponding constant) could be fitted in a reasonable energy range to represent the partial (with certain

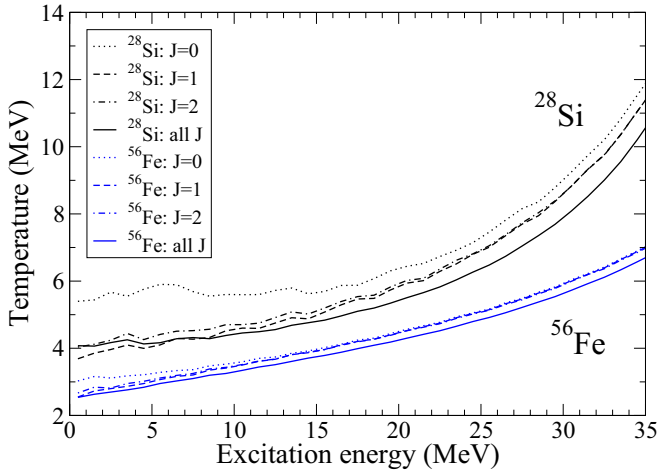

FIG. 11. Thermodynamic temperature as a function of excitation energy, Eq. (18), calculated in the moments method for ^{28}Si, top four curves (black color), and for ^{56}Fe, the bottom four curves (blue color).

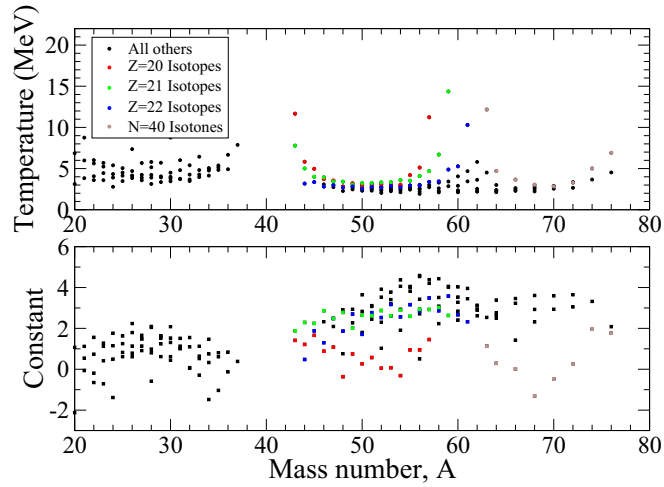

FIG. 12. The constant temperature T and the *constant* [see Eq. (19)] fitted for the energy range 5–15 MeV. Different sets of nuclei from the pf shell with complete and almost complete shells are presented by different colors: $Z = 20$ (red), $Z = 21$ (green), $Z = 22$ (blue), and $N = 40$ (brown).

spin and parity) or total nuclear level densities as

$$\ln[\rho(E,J)] = \frac{E}{T_J} + \text{constant},$$
$$\ln[\rho(E)] = \frac{E}{T} + \text{constant}. \quad (19)$$

It is immediately clear that the constant temperature model cannot be compatible globally with our shell-model calculations. In the truncated orbital space the global level density will always look like a Gaussian with the effective temperature (18)

$$T_{\text{eff}} = \frac{\sigma_E^2}{E_c - E}, \quad (20)$$

changing with energy from positive to negative values on different sides of the centroid energy E_c. Here σ_E is the effective width of the Gaussian that reflects the summed contribution of all components of interactions. However, at relatively low energy the level density can grow approximately exponentially, effectively resulting in an approximately constant temperature.

Here we give a couple of examples showing the exponential fit to the level density of different J classes and global level density. Figure 11 shows how the actual temperature [see Eq. (18)] calculated by the moments method for ^{28}Si and ^{56}Fe depends on the excitation energy. The temperatures calculated for certain spins J and for all spins (the total density) are not constants: they increase with the excitation energy as suggested in Eq. (20). The corresponding constant temperature fit of Eq. (19) performed for the sd and pf nuclei is presented in Fig. 12. The effective constant temperatures in the figure depend on the range of the excitation energies where the fit was performed: the greater the excitation energy the higher the effective constant temperature.

We note that the majority of the fitted temperatures in Figs. 11 and 12 are concentrated in small regions near 2–5 MeV, while there are some exceptional cases of unreasonably high temperatures of 10–20 MeV that correspond to the nuclei with complete or almost complete shells for one or two sorts of nucleons when the Fermi gas approximation is obviously invalid. Finally, Fig. 13 shows how good the constant temperature approximation is. The dotted curve (fitting energy range is 5–15 MeV) and the dashed curve (the range is 5–25 MeV) present the corresponding constant-temperature level densities for ^{28}Si. We can see that these densities work pretty well inside the energy interval where they were fitted compared to the "exact" density calculated within the moments method. As the excitation energy increases, the constant-temperature densities stop working (they rise very high too fast). Figure 14 shows the fitted temperatures when different energy ranges are used: red diamonds present the 1–5 MeV fitting range, black circles and blue squares present 5–15 MeV and 5–25 MeV

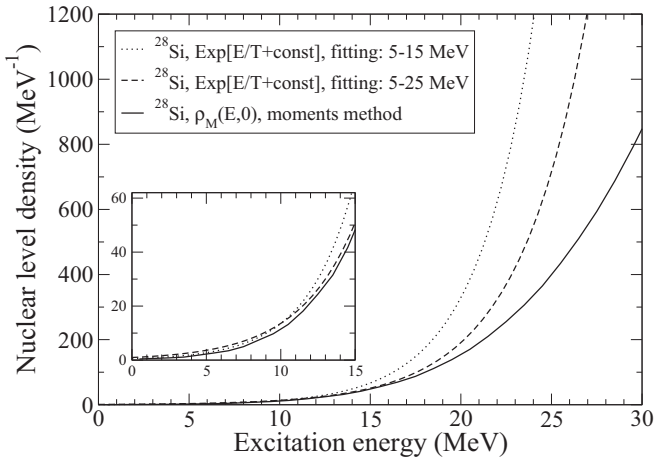

FIG. 13. Comparison between global level densities for ^{28}Si calculated with the moments method (the solid curve) and using the constant temperature for 5–15 MeV (the dotted curve) and for 5–25 MeV (the dashed curve) energy ranges; fits according to Eq. (19). The inset presents the magnified low-energy region.

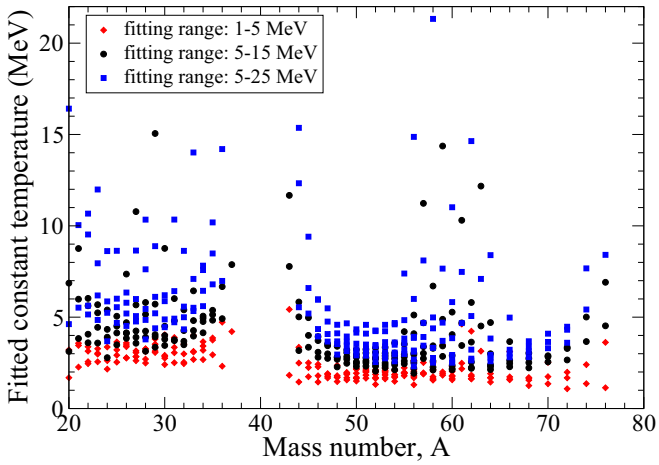

FIG. 14. Constant temperature fitted for *sd* and *pf* shell nuclei. The diamonds (red color) present the fitting range 1–5 MeV, the circles (black color) correspond to 5–15 MeV, and the squares (blue color) correspond to 5–25 MeV.

energy ranges correspondingly. It is natural that at higher excitation energies the effective temperature increases, thus reducing the rate at which the density grows; see Eqs. (19) and (20).

VII. SPIN CUTOFF PARAMETER

The distribution of levels with certain values of global nuclear constants of motion (angular momentum, parity, isospin) is of special interest in all applications. Our method directly supplies the required information for every set of those exact quantum numbers. The standard phenomenological approach to the angular momentum dependence of the level density assumes random angular momentum coupling as a diffusion process in the space of projections M. The total projection results from a random walk, and the fraction of states with a given projection M is Gaussian,

$$\frac{\rho(E,M)}{\rho(E)} = \frac{1}{\sqrt{2\pi\sigma^2}}\, e^{-M^2/2\sigma^2}. \tag{21}$$

Then, as mentioned earlier, the density of states with a given value of J is just a difference

$$\rho_J(E) = \rho(E,M=J) - \rho(E,M=J+1). \tag{22}$$

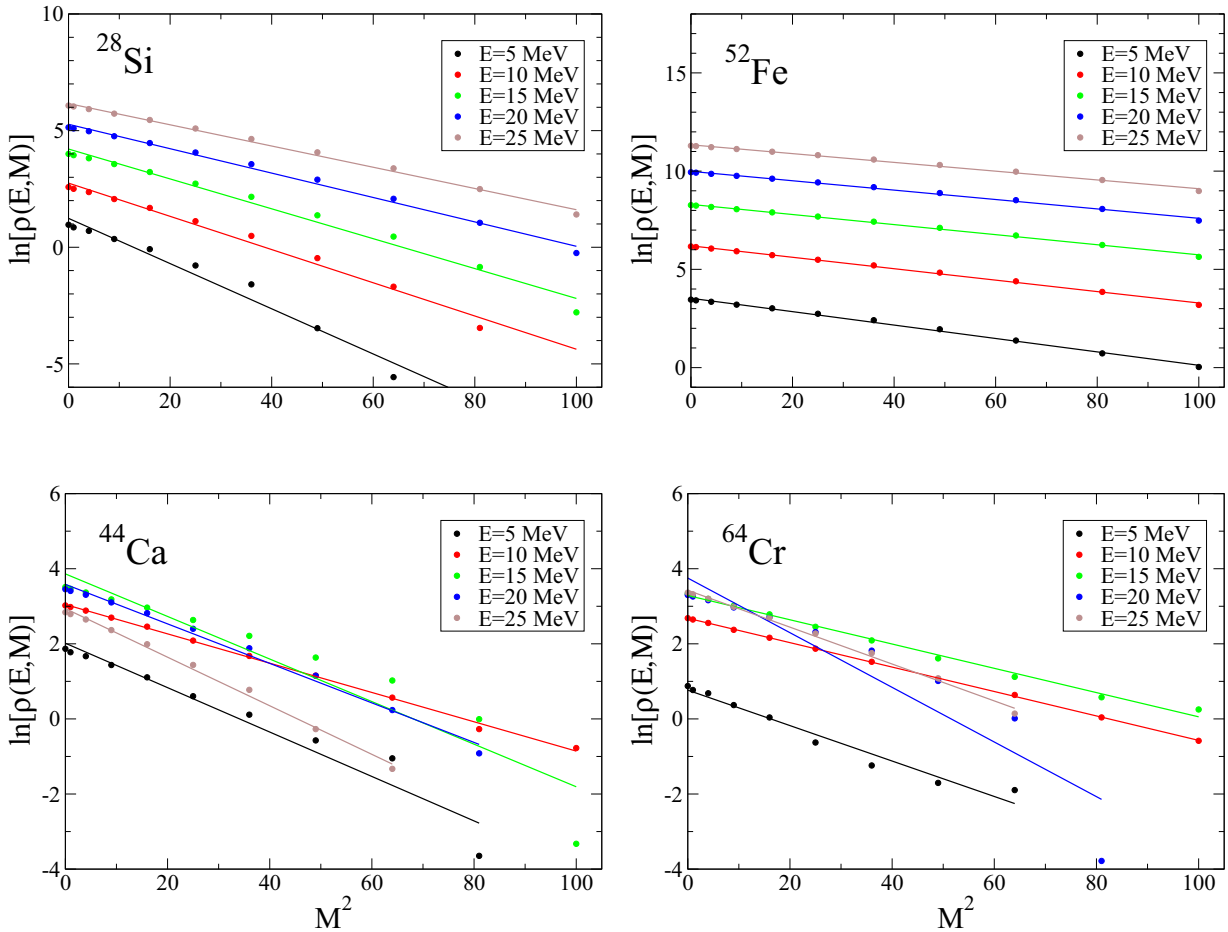

FIG. 15. Logarithm of level density, $\ln[\rho(E,M)]$, versus M^2, Eq. (23), calculated for ^{28}Si, ^{52}Fe, ^{44}Ca, and ^{64}Cr. Different colors present different excitation energies: 5 MeV (black), 10 MeV (red), 15 MeV (green), 20 MeV (blue), and 25 MeV (brown). Dots correspond to the moments method calculations, the solid lines are linear interpolations; see the text.

Assuming this random angular momentum coupling, we expect a linear M^2 dependence of the logarithm of the level density,

$$\ln[\rho(E,M)] = \ln[\rho(E,M=0)] - \frac{M^2}{2\sigma^2}. \qquad (23)$$

The top two graphs of Fig. 15 show the M^2 dependences of $\ln[\rho(E,M)]$ at different energies for ^{28}Si and ^{52}Fe. The lines correspond to the best linear interpolation of this logarithm. In these examples we see a very good linear behavior and the smooth dependence on excitation energy. This can be interpreted as evidence for random coupling of angular momenta of individual particles.

The situation is different in two next examples, the bottom graphs in Fig. 15, ^{44}Ca and ^{64}Cr. Here we do not have a regular energy dependence and, therefore, a clearly defined parameter σ. This is what could be expected from physical arguments. The whole idea of the Gaussian random walk in the angular momentum space breaks down here because of the isospin limitations. The nucleus ^{44}Ca in the shell-model description has only four identical $f_{7/2}$ neutrons, which allow for isospin $T = 2$ only and for the interaction in the particle-particle channel with total isospin $T = 1$. Therefore many values of the total spin are forbidden. The second nucleus, $^{64}_{24}Cr_{40}$, in the pf shell model has only four valence protons with the same limitations of the angular momentum coupling. In both cases, it is hard to expect the requirements of the random spin coupling to be satisfied.

The value of the spin cutoff parameter σ can be extracted from the curves, as in Fig. 15 where we observe a good linear behavior. The first step is to interpolate the shell-model density with a linear function of M^2; see Eq. (23). The obtained slopes in Fig. 15 corresponding to different energies allow us to get the spin cutoff parameter as a function of excitation energy $\sigma^2(E)$. Using thermodynamic language, we expect this parameter to be proportional to temperature, or, for a Fermi-gas, to the square root of energy. The corresponding parametrization can be chosen as

$$\sigma^2 = \alpha\sqrt{E}\,(1 + \beta E). \qquad (24)$$

The coefficient α can be taken [17] from Fermi-gas statistical mechanics as $\propto \nu_F T\langle M^2\rangle$, where ν_F is the single-particle level density at the Fermi surface, or by assuming that the angular momentum corresponds on average to a rigid-body rotation with moment of inertia $\propto TA^{5/3}$. The second step is to interpolate $\sigma^2/\sqrt{E}$ (which we know numerically from the first step) using a linear function of excitation energy E. The results of such a two-step interpolation are shown in Fig. 16. We define the parameters α and β, Eq. (24), from the energy region 5–25 MeV. Comparing two groups of nuclei, sd shell and pf shell, we indeed see the average growth of the spin cutoff parameter for two representative groups being proportional to $A^{5/3}$. It is impossible here to make a selection between the statistical estimate of the spin cutoff parameter and the estimate from the moment of inertia, as both of them, being too crude to reflect shell effects inside each group which are certainly present, do not agree with the $A^{5/3}$ estimate and require a more detailed analysis. The constant β from Eq. (24) is small but, at least for the pf nuclei, may also reflect some shell effects.

Finally, Fig. 17 presents an attempt to compare exact shell-model densities with the Fermi-gas model densities

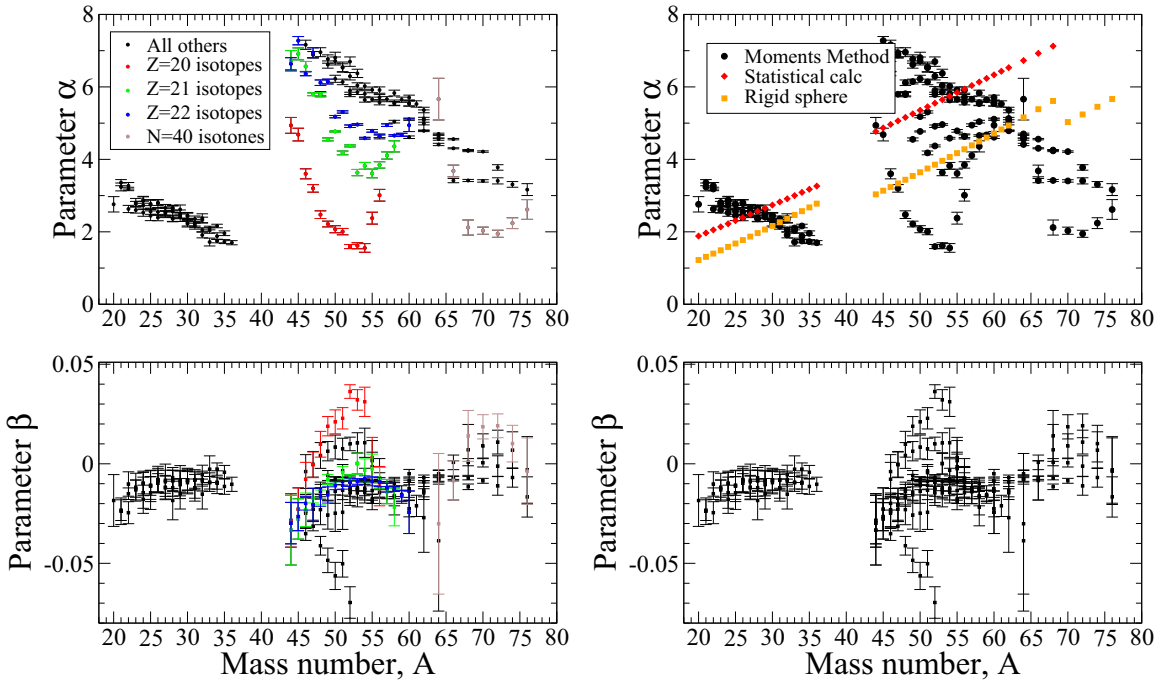

FIG. 16. Interpolation of the spin cutoff parameter σ^2 (see the description in the text for details). Parameters α and β are shown for different sd and pf nuclei. Left panel: different colors present different isotopes or isotones. Right panel: moments method calculation with interpolation (black circles), statistical calculation (orange diamonds), and rigid-body approximation (yellow squares).

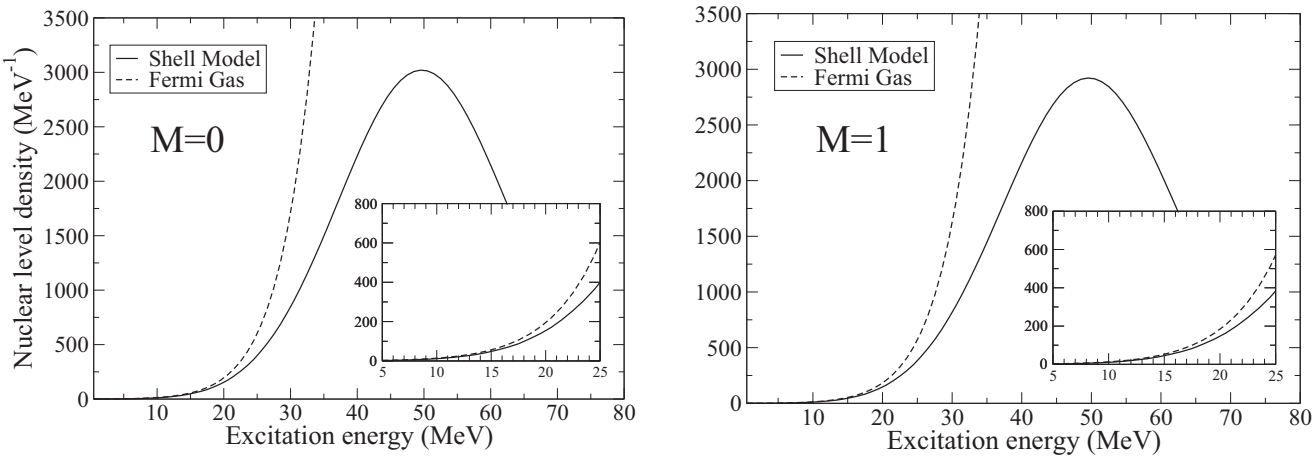

FIG. 17. Partial nuclear level densities for ^{28}Si, $\Pi = +1$, and various spin projections M. The solid curves present the shell model densities (sd shell and USDB two-body interaction [45]) while the dashed curves show the Fermi-gas model densities (with the fitted parameters, see text for details). The insets show the magnified low-energy area that spans from 5 to 25 MeV, where the densities were actually fitted.

calculated with the fitted parameters. For the comparison we picked the ^{28}Si nucleus in the sd model space with the USDB two-body interaction [45]. The plotted Fermi-gas densities combine Eqs. (12), (21), and (24) as

$$\rho_{FG}(E,M) = \frac{1}{E^{5/4}} \exp\left[2\sqrt{aE} + \text{const} - \frac{M^2}{2\sigma^2}\right], \qquad (25)$$

where the spin cutoff parameter is $\sigma^2 = \alpha\sqrt{E}(1+\beta E)$. The fitted parameters are $a = 1.78 \pm 0.03$, const $= -2.92 \pm 0.13$, $\alpha = 2.370 \pm 0.095$, and $\beta = -0.010 \pm 0.003$. We can see that up to 20 MeV, where we still can trust the shell model, the fitted parameters provide a reasonably good agreement between the Fermi gas and shell models. Of course, after a certain energy the Fermi-gas densities go up exponentially while the shell-model densities have to follow a Gaussian-type curve.

VIII. CONCLUSION

In this article we collected, explained, and summarized the first results of an improved method for statistical calculation of the nuclear level density for a given shell-model Hamiltonian. The method is physically based on the chaotization of the intrinsic dynamics by interparticle interactions. In practice, one needs to calculate only the lowest moments of the Hamiltonian partitioned in terms of mean-field configurations. The first two moments turn out to be sufficient for the full agreement of the found level density with the result of the exact diagonalization, as checked by the cases in which such full diagonalization was technically possible. Significant improvements compared to the previous attempts in the same direction include the use of finite-range Gaussian distributions and of the recurrence relation for eliminating spurious states. We did not discuss the determination of the ground state energy, which is necessary for the appropriate positioning of the level density. There are special methods for doing this, including exponential extrapolation also based on the chaotic properties of remote highly excited states [61]. The shell-model level density can be calculated in any specific class of global constants of motion (proton and neutron numbers, total spin, parity, and isospin) as a function of excitation energy. This is essentially what is needed for practical applications to nuclear reactions, including those in astrophysics.

The main conclusion that can be drawn from this experience is that the shell-model level density that results from the statistical calculation is a smooth function of excitation energy in all classes of quantum numbers containing a considerable number of states allowed by the truncation of the orbital space (of course, the state with the maximum possible total spin is unique). Giant oscillations of the level density predicted by calculations based on the mean-field combinatorics are almost completely erased by the presence of incoherent collision-like interactions, which usually remain outside of the mean-field models or parametrizations with the so-called collective enhancement. Taking into account all components of residual interactions, coherent (such as pairing) and incoherent, is necessary for an adequate description. In the same way, one has to study the role of interaction components responsible for the onset of deformation and rearrangement of the spectra by rotational bands.

Comparison with phenomenological Fermi-gas approaches, including models with constant temperature, shows that, although they are less theoretically justified than the full direct calculation, in many cases they are nevertheless quite reasonable for practical use. The calculations of the spin dependence of the level density and of the relevant spin cutoff parameter are more sensitive to assumptions, and there are cases when they are not in good agreement with exact results. The model of constant temperature, in our opinion, can be applied at relatively low excitation energy but, most probably, it reflects the general process of chaotization of the dynamics rather than just breaking of Cooper pairs. Certainly, the accumulation of experimental data and new applications of the statistical method are necessary to better understand the underlying physics.

The whole approach unavoidably suffers from the general problems of the shell model. It is conceivable that the results will not be sensitive to the specific version of the shell-model

Hamiltonian when this choice agrees well with the low-lying spectroscopy. However, the space truncation provides a natural limitation on the applications of all such methods. The space can be expanded (and many-body residual interactions can be included) by paying the price of longer computational time that can be cut off by the parallelization. Regardless, for any choice of finite space there is a natural limit of applicability. Luckily enough, it seems that this limitation is not essential for many astrophysical applications. More theoretical work is necessary to understand the resonance density for the states deep in the continuum, which again might not be critical for a typical stellar temperature when the resonance states under consideration still are quite narrow.

ACKNOWLEDGMENTS

The whole development of the method was done in collaboration with M. Horoi. Discussions with B.A. Brown are acknowledged. The work on level density was supported by the NSF Grants No. PHY-1068217 and No. PHY-1404442.

[1] A. Schiller *et al.*, Nucl. Instrum. Methods Phys. Res., Sect. A **447**, 498 (2000).
[2] A. V. Voinov, S. M. Grimes, C. R. Brune, M. J. Hornish, T. N. Massey, and A. Salas, Phys. Rev. C **76**, 044602 (2007).
[3] A. C. Larsen, M. Guttormsen, M. Krtička, E. Běták, A. Bürger, A. Görgen, H. T. Nyhus, J. Rekstad, A. Schiller, S. Siem, H. K. Toft, G. M. Tveten, A. V. Voinov, and K. Wikan, Phys. Rev. C **83**, 034315 (2011).
[4] T. von Egidy and D. Bucurescu, J. Phys. Conf. Ser. **338**, 012028 (2012).
[5] T. Kawano, S. Chiba, and H. Koura, J. Nucl. Sci. Technol. **43**, 1 (2006).
[6] V. Zelevinsky, B. A. Brown, N. Frazier, and M. Horoi, Phys. Rep. **276**, 85 (1996).
[7] I. C. Percival, J. Phys. B **6**, L229 (1973).
[8] J. B. French and K. F. Ratcliff, Phys. Rev. C **3**, 94 (1971).
[9] S. S. M. Wong, *Nuclear Statistical Spectroscopy* (Oxford University Press, Oxford. 1986).
[10] *Spectral Distributions in Nuclei and Statistical Spectroscopy* edited by V. K. B. Kota and R. U. Haq (World Scientific, Singapore, 2010).
[11] T. A. Brody, J. Flores, J. B. French, P. A. Mello, A. Pandey, and S. S. M. Wong, Rev. Mod. Phys. **53**, 385 (1981).
[12] S. M. Grimes, S. D. Bloom, R. F. Hausman, and B. J. Dalton, Phys. Rev. C **19**, 2378 (1979).
[13] C. W. Johnson, J.-U. Nabi, and W. E. Ormand, arXiv:nucl-th/0105041.
[14] R. A. Sen'kov, M. Horoi, and V. G. Zelevinsky, Phys. Lett. B **702**, 413 (2011).
[15] R. A. Sen'kov, M. Horoi, and V. G. Zelevinsky, Comput. Phys. Commun. **184**, 215 (2013).
[16] H. A. Bethe, Phys. Rev. **50**, 332 (1936); Rev. Mod. Phys. **9**, 69 (1937).
[17] T. Ericson, Adv. Phys. **9**, 425 (1960).
[18] A. Gilbert and A. G. W. Cameron, Can. J. Phys. **43**, 1446 (1965).
[19] H. Baba, Nucl. Phys. A **159**, 625 (1970).
[20] J. A. Holmes, S. E. Woosley, W. A. Fowler, and B. A. Zimmerman, At. Data Nucl. Data Tables **18**, 305 (1976).
[21] C. A. Engelbrecht and J. R. Engelbrecht, Ann. Phys. (N.Y.) **207**, 1 (1991).
[22] A. Bohr and B. Mottelson, *Nuclear Structure*, Vol. 1 (1969), Vol. 2 (1975) (Benjamin, New York).
[23] S. Goriely, S. Hilaire, and A. J. Koning, Phys. Rev. C **78**, 064307 (2008).
[24] H. Uhrenholt, S. Åberg, P. Moeller, and T. Ichikawa, arXiv:0901.1987.
[25] S. Hilaire, M. Girod, S. Goriely, and A. J. Koning, Phys. Rev. C **86**, 064317 (2012).
[26] Y. Alhassid, G. F. Bertsch, S. Liu, and H. Nakada, Phys. Rev. Lett. **84**, 4313 (2000).
[27] Y. Alhassid, S. Liu, and H. Nakada, Phys. Rev. Lett. **99**, 162504 (2007).
[28] Y. Alhassid, A. Mukherjee, H. Nakada, and C. Ozen, J. Phys.: Conf. Ser. **403**, 012012 (2012).
[29] Ya. I. Frenkel, Sov. Phys. **9**, 533 (1936).
[30] L. D. Landau, J. Exp. Theor. Phys. **7**, 819 (1937).
[31] V. V. Flambaum, A. A. Gribakina, G. F. Gribakin, and M. G. Kozlov, Phys. Rev. A **50**, 267 (1994).
[32] V. V. Flambaum and F. M. Izrailev, Phys. Rev. E **56**, 5144 (1997).
[33] V. Zelevinsky, Annu. Rev. Nucl. Part. Phys. **46**, 237 (1996).
[34] L. D. Landau and E. M. Lifshitz, *Statistical Physics* (Pergamon Press, Oxford, 1958).
[35] M. Srednicki, Phys. Rev. E **50**, 888 (1994).
[36] A. Polkovnikov, K. Sengupta, A. Silva, and M. Vengalattore, Rev. Mod. Phys. **83**, 863 (2011).
[37] S. T. Belyaev and V. G. Zelevinsky, Sov. J. Nucl. Phys. **11**, 416 (1970).
[38] N. Pillet, V. G. Zelevinsky, M. Dupuis, J.-F. Berger, and J. M. Daugas, Phys. Rev. C **85**, 044315 (2012).
[39] M. Horoi, J. Kaiser, and V. Zelevinsky, Phys. Rev. C **67**, 054309 (2003).
[40] R. A. Sen'kov and M. Horoi, Phys. Rev. C **82**, 024304 (2010).
[41] N. Frazier, B. A. Brown, and V. Zelevinsky, Phys. Rev. C **54**, 1665 (1996); reprinted in Ref. [10], p. 557.
[42] M. Horoi and V. Zelevinsky, Phys. Rev. Lett. **98**, 262503 (2007).
[43] C. Jacquemin, Z. Phys. A **303**, 135 (1981).
[44] J. Brenneisen *et al.*, Z. Phys. A **351**, 430 (1995); **352**, 443 (1995).
[45] B. A. Brown and B. H. Wildenthal, Annu. Rev. Nucl. Part. Sci. **38**, 29 (1988).
[46] D. H. Gloeckner and R. D. Lawson, Phys. Lett. B **53**, 313 (1974).
[47] http://www-astro.ulb.ac.be/bruslib/
[48] A. V. Ignatyuk, K. K. Istekov, and G. N. Smirenkin, Sov. J. Nucl. Phys. **29**, 450 (1979).
[49] S. Komarov, R. J. Charity, C. J. Chiara, W. Reviol, D. G. Sarantites, L. G. Sobotka, A. L. Caraley, M. P. Carpenter, and D. Seweryniak, Phys. Rev. C **75**, 064611 (2007).
[50] V. G. Zelevinsky, D. Mulhall, and A. Volya, Phys. At. Nucl. **64**, 525 (2001).
[51] A. Volya, V. Zelevinsky, and B. A. Brown, Phys. Rev. C **65**, 054312 (2002).
[52] J. R. Armstrong, S. Åberg, S. M. Reimann, and V. G. Zelevinsky, Phys. Rev. E **86**, 066204 (2012).

[53] G. Rohr, Z. Phys. A **318**, 299 (1984).
[54] S. I. Al-Quraishi, S. M. Grimes, T. N. Massey, and D. A. Resler, Phys. Rev. C **63**, 065803 (2001).
[55] N. Rosenzweig, Phys. Rev. **108**, 817 (1957).
[56] P. J. Brancazio and A. G. W. Cameron, Can. J. Phys. **47**, 1029 (1969).
[57] A. V. Voinov, B. M. Oginni, S. M. Grimes, C. R. Brune, M. Guttormsen, A. C. Larsen, T. N. Massey, A. Schiller, and S. Siem, Phys. Rev. C **79**, 031301 (2009).
[58] M. Guttormsen, B. Jurado, J. N. Wilson, M. Aiche, L. A. Bernstein, Q. Ducasse, F. Giacoppo, A. Görgen, F. Gunsing, T. W. Hagen, A. C. Larsen, M. Lebois, B. Leniau, T. Renstrøm, S. J. Rose, S. Siem, T. Tornyi, G. M. Tveten, and M. Wiedeking, Phys. Rev. C **88**, 024307 (2013).
[59] M. Guttormsen, L. A. Bernstein, A. Görgen, B. Jurado, S. Siem, M. Aiche, Q. Ducasse, F. Giacoppo, F. Gunsing, T. W. Hagen, A. C. Larsen, M. Lebois, B. Leniau, T. Renstrøm, S. J. Rose, T. G. Tornyi, G. M. Tveten, M. Wiedeking, and J. N. Wilson, Phys. Rev. C **89**, 014302 (2014).
[60] L. G. Moretto, A. C. Larsen, F. Giacoppo, M. S. Guttormsen, and S. Siem, J. Phys.: Conf. Ser. **580**, 012048 (2015).
[61] M. Horoi, A. Volya, and V. Zelevinsky, Phys. Rev. Lett. **82**, 2064 (1999); M. Horoi, B. A. Brown, and V. Zelevinsky, Phys. Rev. C **65**, 027303 (2002).